Laser pulses for coherent xuv Raman excitation

Loren Greenman, Christiane P. Koch, and K. Birgitta Whaley

Phys. Rev. A **92**, 013407 — Published 13 July 2015

DOI: 10.1103/PhysRevA.92.013407

Laser pulses for coherent xuv Raman excitation

Loren Greenman,[1, 2] Christiane P. Koch,[3] and K. Birgitta Whaley[1, 2, *]
[1]*Department of Chemistry and Kenneth S. Pitzer Center for Theoretical Chemistry,*
University of California, Berkeley, CA 94720, USA
[2]*Chemical Sciences, Lawrence Berkeley National Laboratory, Berkeley, CA 94720, USA*
[3]*Theoretische Physik, Universität Kassel, Heinrich-Plett-Str. 40, D-34132 Kassel, Germany*

We combine multi-channel electronic structure theory with quantum optimal control to derive femtosecond time scale Raman pulse sequences that coherently populate a valence excited state. For a neon atom, Raman target populations of up to 13% are obtained. Superpositions of the ground and valence Raman states with a controllable relative phase are found to be reachable with up to 4.5% population and phase control facilitated by the pump pulse carrier envelope phase. Analysis of the optimized pulse structure reveals a sequential mechanism in which the valence excitation is reached via a fast (femtosecond) population transfer through an intermediate resonance state in the continuum rather than avoiding intermediate state population with simultaneous or counterintuitive (STIRAP) pulse sequences. Our results open a route to coupling valence excitations and core-hole excitations in molecules and aggregates that locally address specific atoms and represent the first step towards realization of multidimensional spectroscopy in the xuv and x-ray regimes.

I. INTRODUCTION

Multidimensional spectroscopy in the infrared [1] and uv-vis [2, 3] spectral regions has proven to be a powerful tool for revealing quantum coherent dynamics in biological systems [4] and quantum devices [5–7]. Extending the techniques of multidimensional spectroscopy to the xuv and x-ray regimes could open the door to studying energy transfer between different atomic sites in molecules [8, 9]. It would provide a local probe of valence excitations, which would be invaluable for studies of energy transfer processes in biological systems and quantum devices. However, this presents novel challenges, since the large energy of the xuv and x-ray pulses can result in a high probability of ionization, while selective excitation of a specific intermediate state may be hampered by the presence of a multitude of other states closely lying by. On an abstract level, these difficulties reflect the problem of controllability when a continuum of states is involved [10]. Controllability addresses the question whether a quantum control target is reachable, given the properties of the Hamiltonian [11]. For a structureless continuum, no significant controllability is expected, whereas resonances in the continuum are predicted to facilitate control [12], the extent of which depends on the resonance lifetime compared to the duration of the pulses.

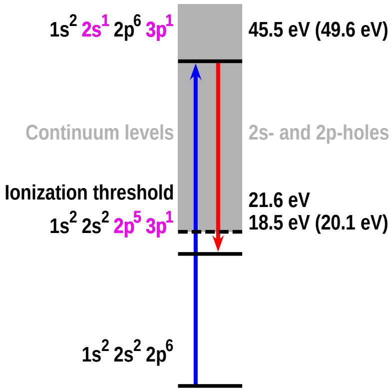

FIG. 1: (Color online) Targeted coherent xuv Raman process in neon. The experimental energies are shown together with TDCIS values in parentheses.

Here we combine quantum optimal control theory with the time-dependent configuration interaction singles (TDCIS) description of electronic structure to calculate experimentally feasible pulse sequences with flexible parameters that coherently excite an xuv Raman excitation on a femtosecond time scale, as a first step towards multidimensional spectroscopy in the x-ray regime [8]. Achieving such coherent Raman excitation with a high yield is extremely challenging, due to the presence of the ionization continuum that is accessible by both pump and Stokes pulses. Furthermore, in order to probe electronic dynamics of valence excitations in molecules, it is imperative to not only transfer population into the excited states, but also to have the capability to prepare coherent superpositions of valence states. We seek thus to both drive population to a specific atomic valence excitation *and* achieve a coherent superposition of ground state and valence excitation with controllable relative phase. We demonstrate here that use of optimal control theory allows prediction of experimentally feasible pulse forms that populate the desired state up to 13% and achieve superpositions of ground and excited state with arbitary relative phase and up to 4.5% excited state population. This work is the first to tackle the problem of an electronic continuum with optimal control, adding an important capability to the growing attempts now underway to tailor multi-electron dynamics [13–16].

We consider as a specific example the neon atom, employing the levels shown in Fig. 1. These are accessible in table-top experiments generating intense high harmonics [17] or using a free-electron laser operating in the xuv

---

[*] Electronic address: `whaley@berkeley.edu`

regime. A pump pulse of 45.5 eV couples the ground state, with configuration $1s^2 2s^2 2p^6$, to the core-excited resonance ($1s^2 2s^1 2p^6 3p^1$), driving a $2s - 3p$ hole-particle excitation. A Stokes pulse of 27.0 eV induces the filling of the $2s$ hole with a $2p$ valence electron, creating the $2p - 3p$ excitation ($1s^2 2s^2 2p^5 3p^1$) which is the target valence excited sate. Although we do not place any restrictions on the pulse form or frequencies, we use the frequencies mentioned above as the starting point for optimization and find that they remain largely unchanged in the optimization. It is therefore the sequence of the pulses that is the key to avoiding ionization during the time required to achieve the valence excitation, while the generation of coherent superpositions of ground and valence excited states is found to be controlled by the carrier phase envelope of the pump pulse. We provide a physical interpretation of the mechanism implied by the optimal pulses in Section III B.

II. THEORY

A. Time-dependent configuration interaction singles method for electronic dynamics including ionization

In order to describe the manifold of excited states and capture the ionizing electron density, we calculate the quantum dynamics using the time-dependent configuration interaction singles (TDCIS) method on a numerical grid with a complex absorbing potential (CAP) [18, 19]. The TDCIS method was developed to capture channel coupling in high harmonic generation [18, 20], and it has been used to describe multichannel dynamics in a number of ultrafast processes [21–24]. The wavepacket is described by a single-determinant Hartree-Fock ground state $|\Phi_0\rangle$, single-particle excitations from occupied orbital i to unoccupied orbital a $|\Phi_i^a\rangle$, and time-dependent coefficients α,

$$|\Psi(t)\rangle = \alpha_0(t)|\Phi_0\rangle + \sum_{i,a} \alpha_i^a(t)|\Phi_i^a\rangle. \tag{1}$$

The dynamical equations for the coefficients are obtained by inserting Eq. (1) into the Schrödinger equation [18]. A complex absorbing potential (CAP) is added to the Hamiltonian in order to capture ionization [18, 25, 26].

We may simplify the electronic structure calculation by employing a Hartree-Fock-Slater one-electron potential as a starting point (TDCIS-HFS). Dynamical calculations with TDCIS-HFS are found to yield final state populations agreeing with full TDCIS results to within a factor of three. A further gain in efficiency is possible by using a simplified configuration space including only ionization levels reachable by one-photon absorption within a bandwidth of a few eV (TDCIS-HFS-1P). Pulse sequence optimizations were performed using the TDCIS-HFS-1P method, and propagations were performed with the optimal pulses at the full TDCIS level. All calculations employed 1000 grid points in 63.6 Å, with a CAP radius of 42.4 Å and CAP strength of 10^{-4}, with angular momentum functions restricted to $L \leq 3$.

B. Optimal pulse design using Krotov's method

Krotov's optimal control method [27–32] is utilized to find pulses which suppress ionization. It minimizes the cost function J for the desired excitation,

$$J\,(t_f) = -|\langle\Phi_D|\Psi(t_f)\rangle|^2, \tag{2}$$

where $|\Phi_D\rangle$ represents the target state (the 2p-3p excitation) and $\Psi(t_f)$ the time evolved state in presence of the external field $\mathcal{E}(t)$. The Krotov pulse update formula is given by [32]

$$\mathcal{E}(t)^{(k+1)} = \mathcal{E}(t)^{(k)} - \frac{\lambda}{2S(t)} \mathrm{Im}\left(\chi(t)^T \mathbf{z} \alpha(t)^{(k+1)}\right), \tag{3}$$

where $\mathcal{E}\,(t)^{(k)}$ is the time-dependent field amplitude at the k-th iteration, $S(t)$ an arbitrary shape function which ensures that the pulse goes to zero at the ends of the time propagation, $\mathbf{z}$ the transition dipole matrix in the basis of TDCIS states, α a vector of the time-dependent coefficients of Eq. (1), and χ the set of corresponding time-dependent co-vectors [29]. The choice of cost function at the final time determines the "initial condition" [29],

$$\chi(t_f) = 2\alpha_D \left(\alpha_D^T \alpha(t_f)\right)^* . \tag{4}$$

The covectors $\chi(t)$ are propagated backwards in time according to the equations of motion,

$$\dot{\chi} = i\left(\mathbf{H}^T - \mathcal{E}(t)^{(k)} \mathbf{z}^T\right)\chi(t)\,, \tag{5}$$

with $\mathbf{H}$ the time-independent part of the Hamiltonian [37]. A derivation of the Krotov update equations is given in the Appendix.

III. RESULTS AND DISCUSSION

A. Obtaining the optimal pulse sequence

Our starting point is a naive pulse sequence for the Raman process obtained by assuming simultaneous, transform-limited (TL) pump (p) and Stokes (S) pulses, $\mathcal{E}_{p/S}(t) = \mathcal{E}_{0,p/S} \sin(\omega_{p/S}(t - t_{0,p/S}) + \phi_{p/S}) \exp[-4 \ln 2 (t - t_{0,p/S})^2/\sigma_{p/S}^2]$, with parameters corresponding to the experimental setup of Ref. [17]: a full-width at half maximum (FWHM) duration of 2 fs and a peak intensity of 3.5×10^{12} W/cm^2. This sequence does not populate the Raman state significantly, cf. Fig. 2(c). The overall depopulation of the ground state is small, of order 10^{-3}. This population is divided between 2p holes

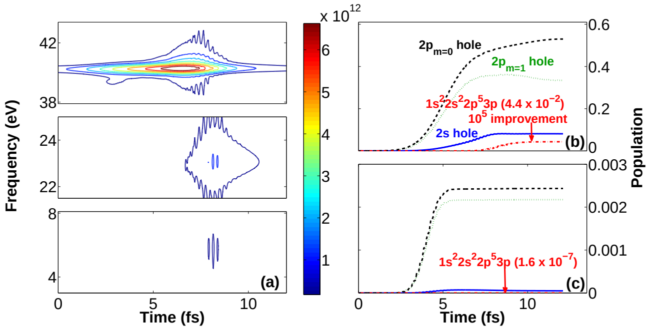

FIG. 2: (Color online) a) Filtered Wigner distribution of the optimized pulse sequence, showing the Stokes pulse starting at the end of the pump pulse and addition of low frequency (eV) components. Color bar units are W/cm^2. (b) Populations of 2p, 2s hole states and the target $1s^22s^22p^53p$ state that are achieved with the optimized pulse. c) Populations for two simultaneous 2 fs TL pulses with central frequencies of 49.6 eV and 29.5 eV. The population of the target state (dashed-dotted red line) reaches 4.4×10^{-2} for the optimized pulse, compared to $\sim 1.6 \times 10^{-7}$ for the naive sequence. The 2p holes ($m = 0$; black dashed line, $m = 1$; green dotted line) correspond to $1s^22s^22p^5nl$ configurations, the 2s hole (blue solid line) to $1s^22s^12p^6nl$ configurations.

and the 2s hole. The target state is a particular configuration of the 2p hole which is populated only to a few hundredths of a percent of the total hole population.

Starting with the naive pulse sequence, an optimized sequence is obtained using Krotov's method. The resulting pulses, shown in Fig. 2(a), achieve the Raman excitation with a population of 4.4×10^{-2}, five orders of magnitude better than the starting pulse. The optimized pulse is increased in amplitude by a factor of about 16 and therefore ionizes more of the electron density. It nevertheless yields an improvement of three orders of magnitude in the percentage contribution of the target state to the total hole probability. The peak intensity of the optimal sequence is about 7.9×10^{14} W/cm^2. Analysis of the dynamics under the optimized pulse reveals the added low frequency contribution (Fig. 2(a)) to be irrelevant, whereas the relative timing of the pump and Stokes pulse components are key features. As discussed below, this suggests a sequential mechanism that may be used to further optimize the pulse sequence within experimental constraints.

Coherent superpositions of the Raman state with the ground state are obtained by optimizing with $0.99e^{i\phi(t)}|1s^22s^22p^53p\rangle + 0.16|1s^22s^22p^6\rangle$ as target state in the cost function (2), where $\phi(t)$ is the desired relative phase. The target state was empirically determined to drive population to the Raman excited state while maintaining the target phase with the ground state. In this optimization, both amplitude and phase of the pulse sequence are varied. The procedure enables identification of pulses for arbitrary, prespecified values of the target phase $\phi(t)$. Figure 3(a) shows the phase error in the target state as a function of $\phi(t)$. The optimized pulses have a combined peak intensity of about 10^{14} W/cm^2 and excite a Raman population of 4.5% while depopulating the ground state by about 53%. Independent of the value of $\phi(t)$, all optimizations are found to converge on the same pulse envelopes that strongly resemble a time-separated pump and Stokes pair, with the Stokes pulse starting just after the peak of the pump pulse, cf. Fig. 3(c). The optimized pulses differ primarily in the value of the carrier envelope phase (CEP) of the pump component, ϕ_p, calculated using a Hilbert transform of the pulse [33]. It is found to correlate closely with the target phase $\phi(t)$, cf. Fig. 3(b). The correlation between target phase and pump CEP implies that the pump imprints its CEP onto the intermediate state to yield the desired relative phase between intermediate and Raman state. These results show that a coherent superposition can be excited with any desired relative phase $\phi(t)$ merely by changing the pump pulse CEP ϕ_p, once the optimized pulse envelope has been determined.

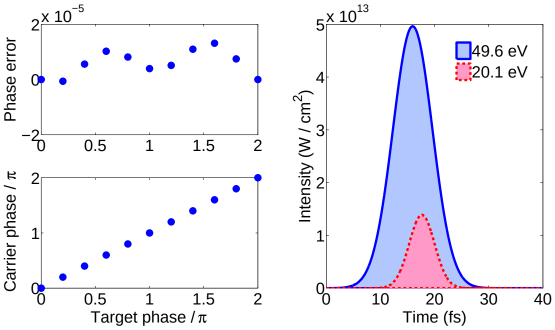

FIG. 3: (Color online) Optimization of coherent superpositions of ground and valence excited states. Phase error (top left panel) and optimized pump pulse carrier envelope phase ϕ_p (bottom left panel), shown as a function of the target phase $\phi(t)$. Right panel: Optimized pulse envelope, showing a clear distinction between pump (earlier) and Stokes (later) component.

Our optimal control calculations suggest a sequential mechanism whereby first the intermediate state is populated and then the second pulse component acts to transfer population and phase information to the desired state. Exploiting this intuition, the pulse sequences can be engineered further by optimizing each step individually, in order to (i) explore large areas of pulse parameter space for maximum performance or (ii) obtain simple pulses with near-optimal performance that are also consistent with experimental constraints. Varying the parameters of a Gaussian-shaped Stokes pulse starting from the intermediate state, we find complete population transfer to the valence state for a pulse duration of 0.5 fs and a peak intensity of 2.4×10^{15} W/cm^2, corresponding to a pulse energy of 0.71 μJ for a spot size diameter of 10 μm. Longer Stokes pulses perform similarly well: Complete population transfer is also achieved by 5 fs and 30 fs pulses with peak intensities of 3.4×10^{13} and 3.3×10^{9} W/cm^2, corre-

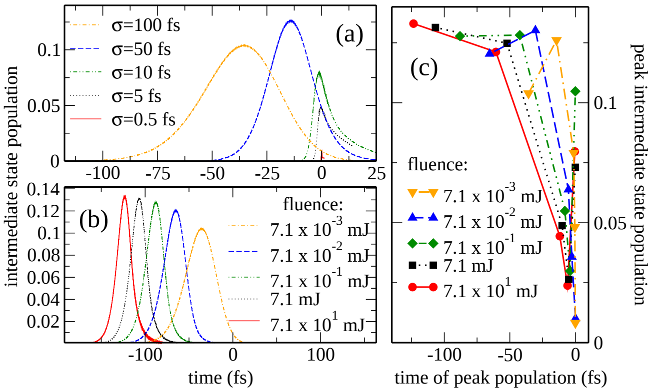

FIG. 4: (Color online) Exploring the performance of Gaussian pump pulses: Intermediate state population as a function of time ($t_{0,p} = 0$) for (a) different pulse durations at a pulse energy of 7.1 μJ, and (b) different pulse energies for a FWHM of 100 fs. As pulse duration increases, larger intermediate state populations can be achieved, although for a given energy the finite lifetime acts to drive the intermediate state population down. (c) Peak intermediate state population as a function of the time it is achieved for different pulse energies (propagations with TDCIS-HFS-1P).

sponding to powers of 0.10 μJ and 0.02 μJ, respectively. Populating the intermediate state efficiently by the pump pulse is thus identified to be the limiting step.

The performance of the pump step is analyzed in Fig. 4 for Gaussian pulses with different pulse durations (a) and energies (b): At a given energy, the maximum intermediate state population first increases with pulse duration ($\sigma \leq 50$ fs). This is explained by a better selectivity of longer, i.e., spectrally narrower pulses, which avoid populating other resonances nearby. However, for very long pulses, the maximum intermediate state population decreases due to the lifetime of the intermediate state, which is about 25 fs [34]. Increasing the pulse energy for a given duration moves the intermediate state population maximum to earlier times and achieves larger maxima for a duration of 100 fs. However, for the smaller powers considered, increasing the pulse duration can lead to a decrease in the population maximum (Fig. 4(c)). The best compromise in terms of pulse power and performance is found for a 50 fs/71 μJ pulse (with peak intensity of 2.4×10^{15} W/cm^2) which achieves a maximum intermediate state population of 0.130, only slightly smaller than the peak at 0.133 seen in Fig. 4(b) for a 100 fs/71 mJ (1.2×10^{18} W/cm^2) pulse.

Improved pulse sequences may now be obtained by setting the Stokes pulse maximum to coincide with the maximum intermediate state population, using pump pulses that balance the incidental transfer to undesired states with the loss due to the intermediate state lifetime. An example is shown in Fig. 5 for a 10 fs pump pulse, yielding a Raman state population of 4.5%, compared to the 7.9% maximum intermediate state population (full TDCIS propagation). When increasing the pump duration to 50 fs, keeping pump energy and Stokes duration and energy fixed, we find final target populations of 13% (using TDCIS-HFS-1P). Such pump pulse parameters are feasible at free electron laser (FEL) facilities where it might prove difficult to realize sub-femtosecond Stokes pulses, however, but longer Stokes pulses may be employed as discussed above.

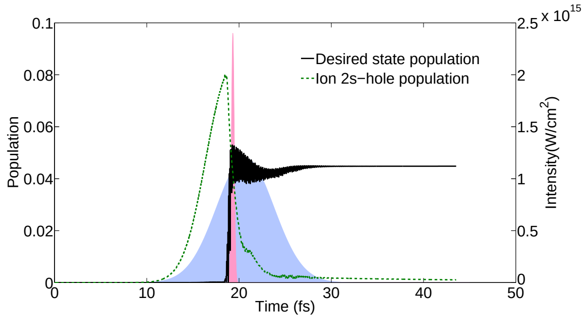

FIG. 5: (Color online) 2s hole population (dashed green line), corresponding mainly to the intermediate state, and target state populations (solid black line) for a 10 fs/7.1 μJ pump pulse and a 0.5 fs/0.71 μJ Stokes pulse centered at 18.7 fs (peak intensities of 1.2 and 2.4×10^{15} W/cm^2, respectively). Pulse sequences are shown in light blue (pump) and red (Stokes).

B. Physical analysis of the optimal pulses

Our optimization reveals that an efficient way to achieve valence excitation is to populate first an intermediate resonance state and then transfer that population to the desired valence excitation. The frequencies of this sequential pair of pulses, as expected, correspond to the resonant frequencies of the intermediate and desired states. To achieve the first goal of populating a valence excited state it is therefore the sequence of the pulses that is the main contribution of the optimal control. The timing of the Stokes pulse starting just before the peak of the pump pulse gives the minimal amount of ionization over the timescale for valence excitation. The optimal control calculations also reveal that the phase of the first, pump pulse is imprinted on the transient population in the intermediate state, which is then transferred to the Raman state by the Stokes pulse.

The simplicity of our optimal pump-Stokes sequences raises the question whether other commonly used schemes for Raman transfer perform equally well. In particular, we may compare with both a simultaneous pair of pump and Stokes pulses, and with a stimulated Raman adiabatic passage (STIRAP) scheme. However neither of these provide comparable performance, as we now discuss.

The key control of relative timing of pulses is lost with simultaneous pulse pairs and they also do not provide the phase control needed to reach arbitrary superposition states. Nevertheless, simultaneous pulses might be expected to allow generation of a high degree of Raman excitation when the pulse amplitudes are increased. We find however that increasing the amplitudes for a set of simultaneous pulses achieves target populations of 0.2% at most, for a pulse intensity of $10^{16}\,\mathrm{W/cm^2}$, before both ionization and competing population transfer to other states take over and the target populations fall again. The increased intensity of the simultaneous pulses generates significant population in other states and increases background ionization from the 2p orbitals, which is the primary cause of loss in this Raman process. We thus see that the lack of a time delay between pump and Raman pulses does not allow for optimization of the transient intermediate state population.

In the well-known STIRAP scheme [35] for Raman excitation, the Stokes pulse precedes the pump to avoid population of the intermediate state and thus the detrimental effect of the intermediate state lifetime. However, in this situation where the intermediate state is a core-excited resonance state, there is only a small coupling between the ground and intermediate states, which results in a very slow adiabatic transfer. In the neon example, we find that valence excitation by a STIRAP scheme is possible only when unrealistically long pulses of hundreds of picoseconds to nanoseconds are employed. Thus at the femtosecond timescales relevant to xuv pulses, STIRAP pulses cannot adiabatically transfer population.

The optimal pulse sequence is neither concerted (simultaneous) nor adiabatic, and instead it selectively populates the intermediate state and depopulates this at the correct timescale to successfully compete with autoionization from the intermediate state (which has a timescale of about 25 fs [34]). The sequential pulses are therefore the optimal pulse choices for the relevant experimental timescales.

IV. CONCLUSION

We have studied the coherent xuv Raman excitation of Ne with shaped pulses and we find that a sequential excitation mechanism proceeding via transient population of an intermediate resonant core-excited state that is then stimulated to emit to the target valence excited state is optimal. We identify the limiting step as population of the intermediate resonance from the ground state. A 50 fs, 71 μJ pump pulse populates the intermediate state up to 13%, and this population can be completely transferred to the Raman state with various Stokes pulses, for example with a duration of 0.5 fs and an energy of 0.71 μJ, or 30 fs and 0.02 μJ. The specific pulses that we find to be optimal at this timescale possess several advantages over the common alternative pulse configuration paradigms for Raman excitation. Thus we showed that simultaneous pulses can not sufficiently populate the desired states before coupling to the continuum and higher intensities increase background ionization and other competing processes, while the Stokes-pump timing of a conventional STIRAP scheme requires far longer timescales to be adiabatic and does not give rise to the desired excitations on timescales of a few hundred femtoseconds. In contrast, the optimal sequential pulse configurations are effective in transferring significant population from the ground state to the target valence excitation desired states with realistic field amplitudes within these times.

Most important for the realization of coherent multidimensional spectroscopies, the optimal shaped pulse results show that it is possible to excite a superposition of the Raman and ground states with a controllable relative phase. Here the primary control knob is the carrier envelope phase of the pump pulse. The pulse intensities and durations that we have determined are in principle possible to realize with FELs, in particular with seeded FELs such as FERMI@Elettra that provide the required power and the time resolution to compete with the resonance lifetime [36]. The optimized coherent Raman calculations thus provide design principles for future FELs, especially in regard to the choice of frequencies and phase control, as a prerequisite to implement a multidimensional x-ray spectroscopy scheme.

The sequential pump-Stokes scheme determined from the optimized pulses can readily be applied to other atoms. Indeed, order-of-magnitude estimates of required pulse durations and intensities can be obtained for atoms with isolated resonances, analogous to the 2s-3p resonance utilized here, by comparing the transition dipole strengths with those of neon. More detailed calculations will be required for overlapping resonances, where longer pulses may be required to preferentially address one resonance over the other, or where alternate mechanisms for Raman excitation may arise which utilize both (or many) resonances. The mechanism suggested by this example of Raman excitation for neon atoms should also work well for localized valence excitation within molecules, since the intermediate state is localized (atom-like) and driving the population into this state is the limiting step.

With this demonstration of the key elements of state-selective population transfer and excitation of superposition states and the mechanistic insight gained from the optimal shaping of pulses to reach these states, systematic development of coherent multidimensional spectroscopies capable of probing the dynamics of valence excitations in molecules via localized core-hole excitations, such as pump-probe and coherent x-ray Raman scattering (CXRS) [8], now appear feasible. The present work illustrates the usefulness and promise of the coherent control approach in bringing techniques such as CXRS to fruition under the challenging environment of atomic and molecular ionization continua.

Acknowledgments

The authors would like to thank Michael Goerz and Daniel Reich for assistance with the Krotov control code, and Stefan Pabst and Robin Santra for help with the XCID TDCIS code. Additionally, we would like to acknowledge Xuan Li, Bill McCurdy, Dan Haxton, Giuseppe Sansone, Ali Belkacem and Holger Mueller for helpful discussions. We acknowledge computational resources obtained under NSF award CHE-1048789 and travel assistance provided by NSF international collaboration grant OISE-1158954 and the DAAD. CPK is grateful for financial support by the State Hessen Initiative for the Development of Scientific and Economic Excellence (LOEWE) within the focus project Electron Dynamic of Chiral Systems (ELCH).

Appendix: Derivation of the Krotov pulse update equations including ionization

We desire to optimize (using the convention of minimization) the overlap of the wavefunction at some time t_f, $|\Psi(t_f)\rangle$, with a desired state $|\Phi_D\rangle$,

$$J_{t_f} = -|(\Phi_D|\Psi\left(t_f\right)\rangle|^2 \tag{A.1}$$

If the desired state is a bound state, the symmetric and Hermitian conjugated overlaps should give the same result because the wavefunction is localized in the CAP-less region and completely real (as in Eq. (2)). In order to simplify the derivation, we first use the final time cost function,

$$\begin{aligned} J_{t_f} &= -\mathrm{Re}\left[(\Phi_D|\Psi\left(t_f\right)\rangle\right], \\ &= -\frac{1}{2}\left[(\Phi_D|\Psi\left(t_f\right)\rangle + (\Phi_D|\Psi\left(t_f\right)\rangle^*\right], \\ &= -\frac{1}{2}\left(\alpha_D^T\alpha\left(t_f\right) + \left(\alpha_D^T\alpha\left(t_f\right)\right)^*\right). \end{aligned} \tag{A.2}$$

We build an optimization functional using the condition in Eq. (A.2), as well as a penalty on the distance of the laser pulse from some reference pulse, and a condition which imposes the TDCIS dynamics using Lagrange multipliers $\chi\left(t\right)$ having the same structure as the coefficient vector $\alpha\left(t\right)$ [27, 28, 30],

$$\begin{aligned} J &= -\frac{1}{2}\left(\alpha_D^T\alpha\left(t_f\right) + c.c.\right) \\ &\quad +\frac{1}{2}\int_0^{t_f}\chi\left(t\right)^T\left(\dot{\alpha}\left(t\right) + i\left(\mathbf{H} - \mathcal{E}\left(t\right)\mathbf{z}\right)\alpha\left(t\right)\right)\mathrm{d}t + c.c. \\ &\quad +\int_0^{t_f}\frac{S\left(t\right)}{\lambda}\left(\mathcal{E}\left(t\right) - \mathcal{E}_{ref,t}\right)^2\mathrm{d}t, \end{aligned} \tag{A.3}$$

where *c.c.* denotes the complex conjugate, a superscript T denotes a transpose, $S\left(t\right)$ is a shape function and λ is an importance parameter for the energy penalty. Integrating the second line of Eq. (A.3) by parts, we obtain:

$$\begin{aligned} \bar{J} &= -\frac{1}{2}\left(\alpha_D^T\alpha\left(t_f\right) - \chi\left(t_f\right)^T\alpha\left(t_f\right) + \chi_0^T\alpha_0 + c.c.\right) \\ &\quad +\frac{1}{2}\int_0^{t_f}\left(-\dot{\chi}\left(t\right)^T\alpha\left(t\right) + i\chi\left(t\right)^T\left(\mathbf{H} - \mathcal{E}\left(t\right)\mathbf{z}\right)\alpha\left(t\right)\right)\mathrm{d}t + c.c. \\ &\quad +\int_0^{t_f}\frac{S\left(t\right)}{\lambda}\left(\mathcal{E}\left(t\right) - \mathcal{E}_{ref}\left(t\right)\right)^2\mathrm{d}t. \end{aligned} \tag{A.4}$$

We desire an update which would guarantee a monotonically decreasing cost function, so we subtract the cost function at iteration $k+1$ from iteration k [27, 28, 30],

$$\bar{J}^{(k+1)} - \bar{J}^{(k)} = -\frac{1}{2}\left(\alpha_D^T\left(\alpha\left(t_f\right)^{(k+1)} - \alpha\left(t_f\right)^{(k)}\right) - \chi\left(t_f\right)^T\left(\alpha\left(t_f\right)^{(k+1)} - \alpha\left(t_f\right)^{(k+1)}\right) + c.c.\right) \tag{A.5a}$$

$$+\frac{1}{2}\left(\int_0^{t_f}\left(-\dot{\chi}\left(t\right)^T\left(\alpha\left(t\right)^{(k+1)} - \alpha\left(t\right)^{(k)}\right) + i\chi\left(t\right)^T\left(\mathbf{H} - \mathcal{E}\left(t\right)^{(k)}\mathbf{z}\right)\left(\alpha\left(t\right)^{(k+1)} - \alpha\left(t\right)^{(k)}\right)\right)\mathrm{d}t + c.c.\right) \tag{A.5b}$$

$$+\int_0^{t_f}\frac{S\left(t\right)}{\lambda}\left(\left(\mathcal{E}\left(t\right)^{(k+1)} - \mathcal{E}_{ref}\left(t\right)\right)^2 - \left(\mathcal{E}\left(t\right)^{(k)} - \mathcal{E}_{ref}\left(t\right)\right)^2\right) + \frac{i}{2}\left(\left(\mathcal{E}\left(t\right)^{(k+1)} - \mathcal{E}\left(t\right)^{(k)}\right)\chi\left(t\right)^t\mathbf{z}\alpha\left(t\right)^{(k+1)} + c.c.\right)\mathrm{d}t. \tag{A.5c}$$

Eq. (A.5) can be ensured to be negative by three conditions. First, Eq. (A.5a) is forced to be zero by setting χ at the final time to be the desired state,

$$\chi\left(t_f\right) = \alpha_D. \tag{A.6}$$

Second, Eq. (A.5b) is set to zero by setting the dynamics of χ,

$$\dot{\chi}\left(t\right) = i\left(\mathbf{H}^T - \mathcal{E}\left(t\right)^{(k)}\mathbf{z}^T\right)\chi\left(t\right). \tag{A.7}$$

Note that Eq. (A.7) depends only on the pulse at the k-th iteration, $\mathcal{E}\left(t\right)^{(k)}$. Finally, to obtain an update, minimize Eq. (A.5c) with respect to $\mathcal{E}\left(t\right)^{(k+1)}$ and allow $\mathcal{E}_{ref}\left(t\right)$ to equal $\mathcal{E}\left(t\right)^{(k)}$ to obtain

$$\mathcal{E}\left(t\right)^{(k+1)} = \mathcal{E}\left(t\right)^{(k)} - \frac{\lambda}{2S\left(t\right)}\mathrm{Im}\left(\chi\left(t\right)^T\mathbf{z}\alpha\left(t\right)^{(k+1)}\right), \tag{A.8}$$

(see Eq. (3)). Note that the update formula depends on the α coefficients at the $(k+1)$-th iteration, and so Eq. (A.8) must be solved self consistently. These update equations are formulated to account for ionization from the CAP in the framework of the TDCIS equations, and like the TDCIS equations they use a symmetric overlap rather than a Hermitian overlap. This also leads to backwards propagation using a transposed Hamiltonian in Eq. (A.7), rather than the Hermitian conjugate.

---

[1] D. S. Larsen, K. Ohta, Q.-H. Xu, M. Cyrier, and G. R. Fleming, J. Chem. Phys. **114**, 8008 (2001).
[2] S. Mukamel, Annu. Rev. Phys. Chem. **51**, 691 (2000).
[3] D. M. Jonas, Annu. Rev. Phys. Chem. **54**, 425 (2003).
[4] G. S. Engel, T. R. Calhoun, E. L. Read, T.-K. Ahn, T. Manl, Y.-C. Cheng, R. E. Blankenship, and G. R. Fleming, Nature **446**, 782 (2007).
[5] X. Li, T. Zhang, C. N. Borca, and S. T. Cundiff, Phys. Rev. Lett. **96**, 057406 (2006).
[6] M. Erementchouk, M. N. Leuenberger, and L. J. Sham, Phys. Rev. B **76**, 115307 (2007).
[7] L. Yang and S. Mukamel, Phys. Rev. B **77**, 075335 (2008).
[8] S. Tanaka and S. Mukamel, Phys. Rev. Lett. **89**, 043001 (2002).
[9] S. Mukamel, D. Abramavicius, L. Yang, W. Zhuang, I. V. Schweigert, and D. V. Voronine, Acc. Chem. Res. **42**, 553 (2009).
[10] M. Shapiro and P. Brumer, Quantum Control of Molecular Processes (Wiley Interscience, 2012).
[11] D. D'Alessandro, Introduction to Quantum Control and Dynamics (Chapman & Hall/CRC, 2007).
[12] V. Zeman, M. Shapiro, and P. Brumer, Phys. Rev. Lett. **92**, 133204 (2004).
[13] T. Klamroth, J. Chem. Phys. **124**, 144310 (2006).
[14] M. Mundt and D. J. Tannor, New J. Phys. **11**, 105038 (2009).
[15] A. Castro, J. Werschnik, and E. K. U. Gross, Phys. Rev. Lett. **109**, 153603 (2012).
[16] X. Li, C. W. McCurdy, and D. J. Haxton, Phys. Rev. A **89**, 031404 (2014).
[17] T. K. Allison, T. W. Wright, A. M. Stooke, C. Khurmi, J. van Tilborg, Y. Liu, R. W. Falcone, and A. Belkacem, Opt. Lett. **35**, 3664 (2010).
[18] L. Greenman, P. J. Ho, S. Pabst, E. Kamarchik, D. A. Mazziotti, and R. Santra, Phys. Rev. A **82**, 023406 (2010).
[19] S. Pabst, L. Greenman, and R. Santra, XCID program package for multichannel ionization dynamics, Rev. 629, with contributions from P. J. Ho. DESY, Hamburg, Germany, 2011.
[20] S. Pabst, L. Greenman, D. A. Mazziotti, and R. Santra, Phys. Rev. A **85**, 023411 (2012).
[21] S. Pabst, L. Greenman, P. J. Ho, D. A. Mazziotti, and R. Santra, Phys. Rev. Lett. **106**, 053003 (2011).
[22] A. Wirth, M. T. Hassan, I. Grguraš, J. Gagnon, A. Moulet, T. Luu, S. Pabst, R. Santra, Z. Alahmed, A. Azzeer, et al., Science **334**, 195 (2011).
[23] S. Pabst, A. Sytcheva, A. Moulet, A. Wirth, E. Goulielmakis, and R. Santra, Phys. Rev. A **86**, 063411 (2012).
[24] A. Sytcheva, S. Pabst, S.-K. Son, and R. Santra, Phys. Rev. A **85**, 023414 (2012).
[25] A. Goldberg and B. W. Shore, J. Phys. B **11**, 3339 (1978).
[26] R. Santra and L. S. Cederbaum, Phys. Rep. **368**, 1 (2002).
[27] D. Tannor, V. Kazakov, and V. Orlov, in Time-dependent quantum molecular dynamics, edited by J. Broeckhove and L. Lathouwers (Plenum, 1992), pp. 347–360.
[28] J. Somlói, V. A. Kazakovski, and D. J. Tannor, Chem. Phys. **172**, 85 (1993).
[29] A. I. Konnov and V. A. Krotov, Automat. Rem. Contr. **60**, 1427 (1999).
[30] A. Bartana, R. Kosloff, and D. J. Tannor, Chem. Phys. **267**, 195 (2001).
[31] J. P. Palao, R. Kosloff, and C. P. Koch, Phys. Rev. A **77**, 063412 (2008).
[32] D. Reich, M. Ndong, and C. P. Koch, J. Chem. Phys. **136**, 104103 (2012).
[33] J. Duoandikoetxea and D. Cruz-Uribe, Fourier analysis (American Mathematical Society, 2001).
[34] K. Codling, R. P. Madden, and D. L. Ederer, Phys. Rev. **155**, 26 (1967).
[35] K. Bergmann, H. Theuer, and B. W. Shore, Rev. Mod. Phys. **70**, 1003 (1998).
[36] `http://www.elettra.trieste.it/FERMI`.
[37] The presence of matrix transposes instead of the usual Hermitian conjugates is due to the use of a CAP.